JOURNAL OF SPACECRAFT AND ROCKETS
Vol. 38, No. 4, July–August 2001

Evolution of Debris Clouds to Microscopically Chaotic Motion

John P. W. Stark*
University of London, London, England E1 4NS, United Kingdom

An evaluation is presented of the effects of orbital perturbations that arise in the early phase of debris cloud evolution. This assessment enables the definition of various characteristic timescales associated with the cloud evolution to a mature debris population, characterized by a "chaotic" distribution, required for the statistical description of debris as provided by the direct simulation Monte Carlo method (DSMC). The influences of gravitational harmonic terms J_2, J_3, and J_4 together with that for solar radiation pressure upon both the precession of the argument of perifocus (resulting in the familiar torus) and regression of the line of nodes (resulting in a band structure) are presented. Dimensionless characteristic timescales indicating the rate at which the evolution in the orbital parameters, subject to each of the perturbations relative to the orbital lifetime, are defined. From this modeling approach to debris studies, it is noted that the dimensionless ratio {perturbation evolutionary timescale} to {orbital lifetime} must be greater than unity. A general conclusion is that it is found that for objects of centimetric size above an altitude of approximately 350 km the DSMC methodology is appropriate. The presented analytic approach highlights the significant influence during the early phase of J_3. The methodology is applied to several scenarios for the fragmentation caused by collisions and explosions. The results show clearly how the evolution to a fully chaotic debris distribution is mass specific and scenario dependent. Debris particles ejected with forward component velocity vectors result with a mass spectrum, which differs from those ejected with rearward velocities. Assumptions of isotropic fragmentation must therefore only be considered as approximations.

Nomenclature

A	=	object cross-sectional area, m^2
a	=	orbit semimajor axis, km
BC	=	ballistic coefficient $C_D \cdot A/m$, m^2/kg
b_e	=	empirical breakup parameter in explosion
C_D	=	drag coefficient, 2.2
$\boldsymbol{c}$	=	debris velocity vector, m/s
c_e	=	empirical breakup parameter in explosion
c_r	=	debris collision relative velocity, m/s
d	=	particle characteristic size, m
E	=	kinetic energy of object collision, J
EMR	=	collision energy per unit mass, J/gm
e	=	orbit eccentricity
$\boldsymbol{F}$	=	external force
f	=	one particle velocity distribution function
i	=	orbit inclination
J_n	=	Earth zonal harmonic term of degree n
k	=	empirical constant
M_t	=	total mass of object, kg
m_c	=	minimum mass for collision induced particle, kg
m_f	=	fragment mass, kg
n	=	number density, m^{-3}
R_e	=	mean radius of Earth, 6378.14 km
T_{char}	=	characteristic time: {orbit lifetime}/{band formation time}
T_r	=	time ratio: {orbit lifetime}/{time for either Ω or ω to evolve through 2π}
t	=	time, s
V_{imp}	=	object relative velocity of collision, m/s
v_c	=	postcollision particle velocity, m/s
ΔV	=	velocity increment in orbital velocity, m/s
$\partial\Omega_n/\partial t$	=	rate of change in Ω caused by J_n, rad/s
$\partial\omega_n/\partial t$	=	rate of change in ω caused by J_n, rad/s
μ	=	Earth gravitational constant, 398,600 km^3/s^2
Ω	=	orbit right ascension of the ascending node, deg
ω	=	orbit argument of perifocus, deg

Subscripts

c	=	collision induced
e	=	explosion induced
g	=	units of mass, g
p	=	projectile
t	=	target

Introduction

A VARIETY of techniques have been developed to model the evolution of space debris. The technique developed at Queen Mary and Westfield (QMW) College has been the novel application of the direct simulation Monte Carlo method (DSMC), originally developed by Bird,[1] to flowfield modeling for rarefied gas dynamics. The QMW approach has recently been fully reported.[2] Early results from this work[3–7] have demonstrated how the technique performs when considering both long-term evolution studies[3,4] and risk assessments.[6,7] The latter paper[7] demonstrated consistency between the predictions of the method and the replacement frequency of shuttle windows.

Fundamental to the DSMC methodology is the assumption of molecular chaos. In the context of debris modeling, this assumption has been interpreted as the debris has lost reference to its specific initial conditions. Realistically such loss requires dispersion in both right ascension of the ascending node Ω and argument of perifocus ω. Evolution can then be considered to have taken place when a differential evolution of 2π in each of these two orbital elements within a dispersing debris cloud has arisen. Clearly this is a less severe condition than a fully chaotic debris environment, which would require the further evolution of the inclination of the orbit plane. This limitation is not, however, significant because our reduced requirement will only result in the lower state-space population density in those physical cells located at high latitude. This under population should however be recognized as occurring in those target orbit planes at high inclination, such as those found for sun-synchronous vehicles.

The purpose of this paper is to address the issue of how well satisfied the debris-chaos assumption is for low Earth orbit (LEO) vehicles and thus to demonstrate the limitations in applicability of the DSMC methodology. The evaluation is undertaken by calculating the characteristic evolution timescales, resulting from the various physical phenomena, which act to perturb the orbit of an object from its initial Keplerian values. The phenomena considered include

Received 5 May 2000; revision received 14 December 2000; accepted for publication 15 February 2001.

*Professor, Department of Engineering, Queen Mary and Westfield College.

the secular effects arising from J_2, J_3, and J_4, together with a simplified approach to solar radiation pressure (SRP), which while having no secular effect upon the orbits considered can influence evolution. This approach to SRP indicates the maximum influence that might be expected from this source. The key issue for the evolving cloud structure in a DSMC methodology is whether there is sufficient time for the differential changes in the orbit parameters to have occurred prior to orbit decay of any specific group of particles. Thus the evolution caused by each of the perturbing forces is compared to the time taken for debris to enter the final rapid phase of orbit decay as a result of atmospheric drag and defined by King-Hele.[8] For the chaotic assumption to be valid, the lifetime must clearly be greater than the evolutionary timescale.

This paper is structured in the following way. A brief synopsis of the DSMC method is provided, identifying the need for a chaotic distribution in velocity space. The methodology used to define the individual perturbations in the context of evolutionary timescales is then given for the first four harmonic terms of the Earth's gravitational field, together with that for SRP. The importance of differential motion in the debris cloud regarding these perturbations is highlighted. Analytic results are then presented to show the broad trends in the evolving structure of the debris cloud. Finally the use of the evolutionary timescale method is used to evaluate the state of fragmentation events occurring at different altitudes, including International Space Station (ISS)-type orbits.

Direct Simulation Methodology for Debris Evaluation

A full description of the underlying methodology of DSMC, applied to rarefied gas dynamics, can be found in Bird.[1] The method solves the Boltzmann equation, which underlies kinetic theory using a computational approach. The methodology separates out the effects of convective transfers in phase space from those arising from scattering. The process is dependent however on the specific assumptions that 1) it is possible to take a statistical sample of the population of particles which are to be modeled (i.e., a Monte Carlo method); 2) it is possible to separate out convective motion from the collision process if an appropriate collision time is defined which accurately represents the statistical nature of collisions within the system of particles; and 3) the individual particles within the system of particles have microscopically chaotic speeds which may be defined by some overall characteristic velocity distribution, as is fundamental to kinetic theory .

The model[2] extends this methodology to the case were the external force field is that representative of the orbital environment.

An issue that has not however been addressed in detail in the literature is the assumption of the microscopically chaotic motion for space debris particles. Evidently, after some initial event that generates debris, there will be a considerable correlation among particles. During this phase of evolution, the trajectories of individual particles can be traced back to their point of origin in phase space. However, after some time has elapsed differential evolution takes place and particles lose their identity with the release event.

What then is the evolutionary timescale for this randomization of the velocity field? Early work on the evolution of debris clouds[9–11] demonstrated that under the influence of J_2 the harmonic term associated with Earth oblateness, a debris cloud once formed would first generate a pulsating ellipsoid[10] before becoming a torus and subsequently a band. It is only after this latter stage that the cloud may be assumed to be dispersed. Results presented[11] showed that during the band formation process the widening of this band by the ensemble of particles does not take place uniformly with a higher density of particles at extreme latitudes. It appears appropriate therefore to define evolution to have taken place only when this band has been completely formed. This assumption has been adopted for the following analysis and is therefore the criterion used to define the evolution to a chaotic state, as required for DSMC modeling.

The issue now to be addressed is for what subset of particles, created in a fragmentation event, will the orbits be sufficiently long lived, for this overall band to form? Clearly in very low orbits the dominance of aerodynamic forces on the particles is such that they will not form a band. However for high Earth and geostationary orbits, for all realistic parameters of the initial state vector of potential debris, the orbit lifetime is very much greater than that associated with band formation. It is clear that the intrinsic time period required for band formation is not the key parameter, rather it is the ratio of the time to form a band relative to the orbit lifetime. In the DSMC model approach[2] characteristic time ratios for groups of particles with specified values for cross-sectional area are considered to probe the chaotic assumption.

Perturbation Modeling

In the LEO region the dominant effects that need to be investigated are those of Earth zonal harmonic terms, SRP, and atmospheric drag. The influences of lunar and solar gravity are omitted from the present analysis because their main influence is upon orbit inclination, which is not the focus of this study.

Earth Zonal Harmonics

The dominant secular effect in LEO arises from the Earth oblateness term J_2. The evolution to a torus and a band requires a progressive drift in right ascension of the ascending node Ω and the argument of perifocus ω. Although higher Earth harmonic terms, i.e., J_n where n is greater than 2, also have secular influences upon other orbital parameters, in this study only these two elements are evaluated.

Various formulisms for the influence of J_2 can be found in the literature, and an appropriate form is the following:

1) Evolution in right ascension of the ascending node Ω (radians per second) caused by J_2:

$$\frac{\partial \Omega_2}{\partial t} = -1.5 \frac{\mu^{0.5} \cdot J_2 \cdot R_e^2 \cdot \cos(i)}{a^{\frac{7}{2}} \cdot (1-e^2)^2} \tag{1}$$

2) The evolution of the argument of perifocus ω (radians per second) caused by J_2:

$$\frac{\partial \omega_2}{\partial t} = 1.5 \frac{\mu^{0.5} \cdot J_2 \cdot R_e^2 \cdot [2 - 2.5 \cdot \sin^2(i)]}{a^{\frac{7}{2}} \cdot (1-e^2)^2} \tag{2}$$

Expressions including the secular effects arising from J_3 and J_4 are more complex but are given in a suitable analytic form by Groves.[12] Modifying these expressions so that they are consistent with current terminology and writing $\partial \Omega_n / \partial t$ as the evolutionary rate caused by the nth harmonic term, etc., they can be written in the following form:

$$\frac{\partial \Omega_3}{\partial t} = \frac{3}{8} \cdot \mu^{0.5} \cdot J_3 \cdot R_e^3 \cdot a^{-\frac{9}{2}} \cdot e \cdot (1-e^2)^{-3} \cdot \cot(i) \times [15 \cdot \sin^2(i) - 4] \cdot \sin(\omega) \tag{3}$$

$$\frac{\partial \Omega_4}{\partial t} = -\frac{3}{14} \cdot \mu^{0.5} \cdot J_4 \cdot R_e^4 \cdot a^{-\frac{11}{2}} \cdot (1-e^2)^{-4} \times \cos(i)\{(1 + 1.5 \cdot e^2) \cdot [7 \cdot \cos^2(i) - 3] - [7 \cdot \cos^2(i) - 4] \cdot e^2 \cdot \cos(2 \cdot \omega)\} \tag{4}$$

$$\frac{\partial \omega_3}{\partial t} = -\frac{3}{8} \cdot \mu^{0.5} \cdot J_3 \cdot R_e^3 \cdot a^{-\frac{7}{2}} \cdot e^{-1} \cdot (1-e^2)^{-3} \cdot \sin(i) \times \{(5 \cdot \cos^2(i) - 1 + e^2 \cdot [35 \cdot \cos^2(i) - 4 \cdot \cos ec^2(i)]\} \cdot \sin(\omega) \tag{5}$$

$$\frac{\partial \omega_4}{\partial t} = \frac{15}{32} \cdot \mu^{0.5} \cdot J_4 \cdot R_e^4 \cdot a^{-\frac{11}{2}} \cdot (1-e^2)^{-4} \cdot (\{[49 \cdot \cos^4(i) - 36 \cdot \cos^2(i) + 3] + 0.75 \cdot e^2 [63 \cdot \cos^4(i) - 42 \cdot \cos^2(i) + 3]\} + \{\sin^2(i) \cdot [7 \cdot \cos^2(i) - 1] - 0.5 \cdot e^2 \times [63 \cdot \cos^4(i) - 56 \cdot \cos^2(i) + 5]\} \cdot \cos(2 \cdot \omega)) \tag{6}$$

Figures 1 and 2 plot the ratios for perturbations J_2:J_3 and J_2:J_4 associated with these gravitational influences upon the rates of evolution

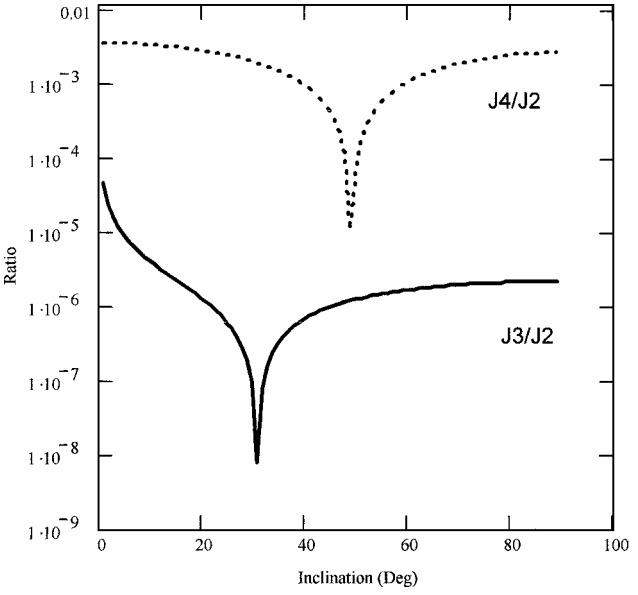

Fig. 1 Regression of the line of nodes: ratio of perturbations J_3/J_2 and J_4/J_2 at 800 km.

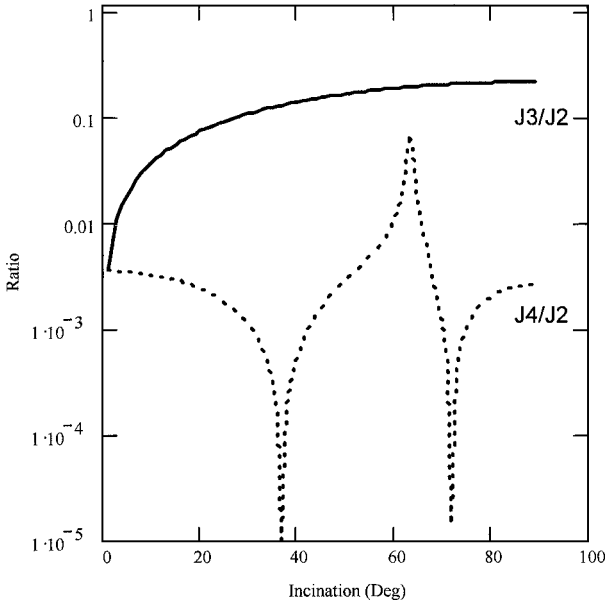

Fig. 2 Precession of the argument of perifocus: ratio of perturbations J_3/J_2 and J_4/J_2 at 800 km.

of ω and Ω for specific orbits. It is apparent that the magnitude of these absolute rates of changes is dominated by the term J_2.

Solar Radiation Pressure

It is not possible to provide simple analytic expressions for the evolution caused by the perturbation arising from SRP upon an orbital object. To provide a detailed evaluation, it is necessary to calculate the influence of SRP during the sunlit portion of the orbit. Aksnes[13] notes that the assumed values for the eccentric anomaly E on entry and exit to eclipse can have a significant influence on the resulting perturbation.

The expressions presented by Aksnes were used to indicate the broad context and the maximum possible rate of evolution as a result of SRP. Representative results are shown in Fig. 3 for the case where the area to mass ratio of the object is 0.025. The equivalent diameter of a spherical aluminum debris particle is 2 cm. The influence of SRP scales directly with area-to-mass ratio or alternatively for spherical particles of constant density, as the reciprocal of diameter.

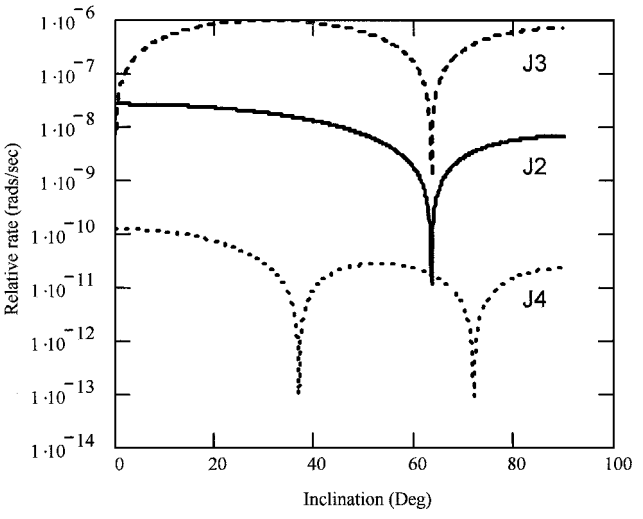

Fig. 3 Differential evolution of perifocal precession caused by the individual effects of J_2, J_3, and J_4 at 800 km.

Lifetime Modeling

The model developed by King-Hele[8] was adopted in this analysis for orbit lifetime evaluation. At a given altitude the most significant influence when considering debris lifetime is the epoch at which the debris cloud is released. Indeed solar activity effects can yield lifetime predictions that differ by two or three orders of magnitude, whereas the effects of other atmospheric parameters, such as oblateness for example, are typically less than 25%.

In the results shown solar activity effects were included via the assumed density scale height at perigee of the orbit. For average solar activity a density of 3.67×10^{-11} kg/m^3 and a density scale height of 67 km were adopted as reference conditions for 200-km altitude.

Relative Evolutionary Timescales

Calculations were performed to determine the ratio of the lifetime (decay time from the original orbit of the object, which followed from the debris injection event) to the timescale for evolution of each of the parameters Ω and ω, subject to each of the perturbations.

Three different measures of evolution were adopted: 1) the time taken for Ω and ω to evolve through 2π radians relative to the initial value of the parameter; 2) the time taken to form a toroidal shell, as described by Housen[9]; and 3) the time taken to form a band, again as described by Housen.

Although more sophisticated models have been developed than those described by Housen, for example McKnight[14] and Jehn,[11] the formulation given by Housen provides a simple analytic expression of the evolving cloud. A crucial concern to the validity of the DSMC methodology is the assumption of evolution in the cloud taking place prior to deorbiting of a debris particle caused by aerodynamic drag. The extent to which evolution will take place is dependent on the dispersion velocity in the fragmentation event. As a consequence, it is appropriate to plot the ratio of evolution timescales, as a function of dispersion velocity.

Analysis is first presented for several generic scenarios. In all cases it has been assumed that the initial parent orbit of the object, prior to fragmentation, is near circular, with an eccentricity of 0.001. For these results dispersion velocity is directed along the instantaneous velocity vector. As a result, only eccentricity and semimajor axis change for the fragmented debris particles.

Evolution Caused by J_2, J_3, and J_4

Figures 1 and 2 show the dominance of J_2 in absolute evolutionary rates of change in Ω and ω. Simply considering the absolute rates is misleading however; when considering the evolution of a debris cloud, it is the differential rates occurring within an ensemble of particles, which is more relevant. Figure 3 shows the differential rate of change of ω (rad/s) as a function of the inclination angle for two orbits, where it has been assumed that a ΔV of 10 m/s has separated two objects and where the initial semimajor axis is

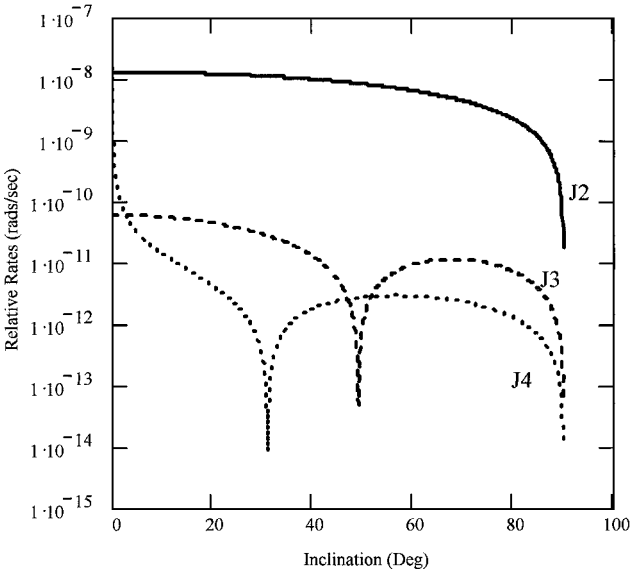

Fig. 4 Differential evolution regression of the line of nodes caused by the individual effects of J_2, J_3, and J_4 at 800 km.

7200 km. The initial orbit was assumed to have an eccentricity of 0.001, and the ΔV is applied at perigee.

The importance of including J_3 is evident. It is also now apparent that there is also a zero in the calculation of the differential rate caused by J_3 close to the critical angle. Around this angle J_4 also needs to be considered, and its effect is shown in Fig. 3. Other than near this critical angle, J_4 is seen to be typically three orders of magnitude below the now predominant J_3 term. Thus for a debris cloud the evolution in argument of perifocus, defining the formation of the toroidal structure must include both the effects of J_3 and J_4 in addition to that of J_2. This to date has been omitted from analytic studies.

The influence of J_3 and J_4 upon the evolution in Right Ascension of the Ascending Node for a differentially evolving debris cloud is shown in Fig. 4. Here the evolution caused by the higher harmonic terms is typically two orders of magnitude below that for the oblateness term. These higher harmonic terms do not therefore add materially to the evaluation of the band formation.

Figure 5 shows the comparison of evolutionary timescales as determined by the time taken for both right ascension (labeled Ω-dot) and argument of perifocus (labeled ω-dot) to precess through 2π radians [i.e., evolution of type 1) as just stated], as a function of the dispersion velocity ΔV for the case of average solar activity and where only the influence of J_2 and J_3 are included. Each of the figures relates to an inclination angle of 30 deg. For these calculations the debris particles released have been assumed to have an area-to-mass ratio of 0.025, equivalent to spherical aluminum particles with a radius of 1 cm. With the characteristic time ratio T_r defined to be the ratio of {the time taken for either Ω or ω to evolve through 2π} to {the orbit lifetime}, a value of T_r greater than unity demonstrates that evolution will have taken place prior to debris decay. From Fig. 5 it is apparent that certainly at 800 km all objects, even those with very small dispersion velocities, will meet this criterion for evolution. Because the lifetime of an object is inversely proportional to area to mass, for spherical uniform density particles a particle larger than 1-cm radius will have a longer lifetime than for the data used in compiling Fig. 5. These larger particles will thus more readily meet the criteria for the characteristic time ratio required for DSMC validation.

Figure 6 provides a summary of results with T_r greater than unity for both high and low solar activity as a function of altitude. For each of the plotted data, a 30-deg inclination is assumed with a particle area-to-mass ratio of 0.025. Because of the scaling of T_r with size, the ΔV requirement for evolution to have occurred is inversely proportional to size; thus, for an aluminum particle of 100-μm radius the ΔV would be required to be 100 times the value shown in Fig. 4.

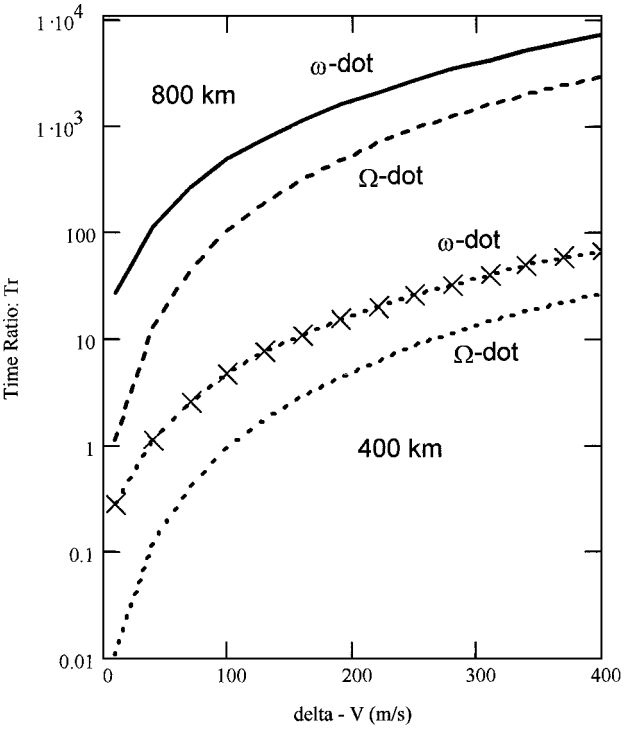

Fig. 5 Time ratio T_r for { the evolution time for specific perturbation} to { orbit life time} as a function of ΔV for average solar activity.

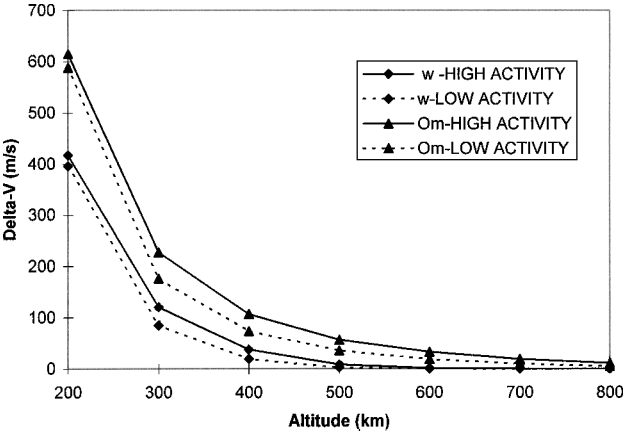

Fig. 6 Required ΔV for T_r >1 as a function of altitude and solar activity.

The time taken for toroidal shell formation, evolution of type 2) and band formation of type 3) only include the influence of J_2. The effect of J_3 is generally to increase the rate at which the formation of the toroidal structure will occur. Figure 7 shows the ratio of times for evolution T_r including and not including J_3. For low velocity dispersion the inclusion of J_3 suggests that the time to form a torus can be an order of magnitude shorter than that estimated in its absence. At high ΔV the absence of J_3 predicts a reduced evolution timescale. This apparent shift is caused by the fact that J_3 and J_2 have an opposite sense of rotation in the argument of perifocus.

Evolution Caused by SRP

Using the model of Aksnes,[13] calculations were performed in a similar manner to those just described for gravitational influences. The results for both precession of the argument of perifocus and the regression of the line of nodes are shown in Figs. 8 and 9. These data are presented as before relative to the lifetime of a particle in the specific orbit. Because of the dependence of both orbital lifetime and perturbation arising from SRP, to a first-order approximation, the effect of ballistic parameter cancels. The data are thus valid for all particle sizes.

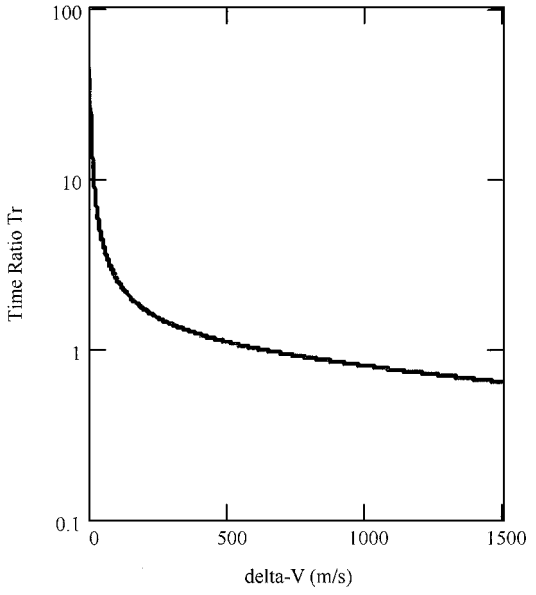

Fig. 7 Ratio of evolution time given by Housen[9] and ω-dot evolution time with J_2 and J_3 included.

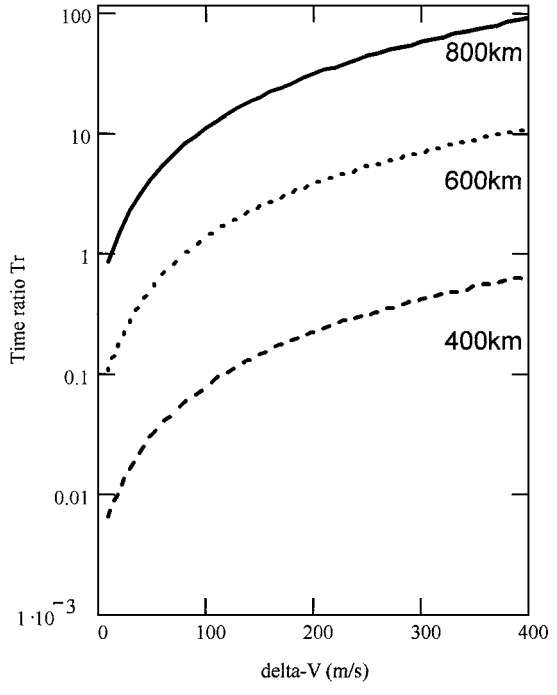

Fig. 8 T_r for evolution in perifocal precession caused by solar radiation pressure alone.

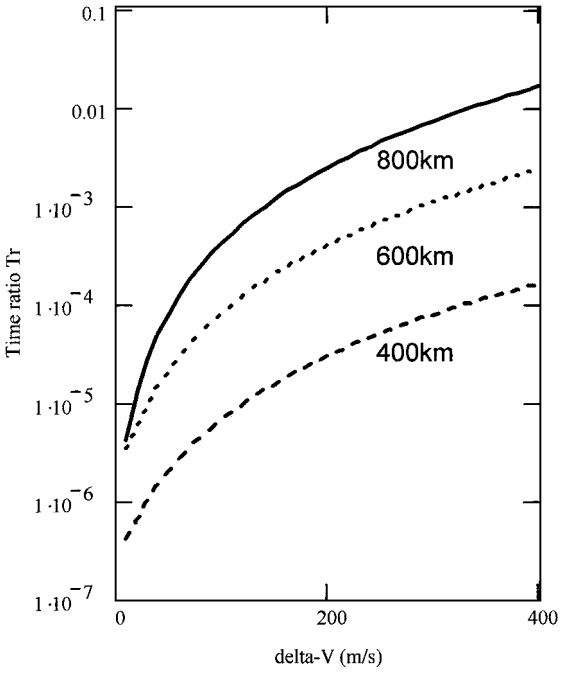

Fig. 9 T_r for evolution in regression of the line of nodes caused by solar radiation pressure alone.

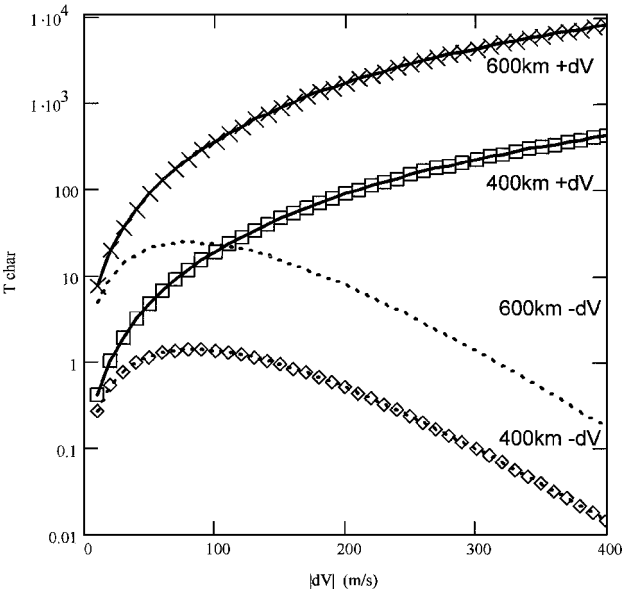

Fig. 10 Values of T_{char} for forward-directed and rearward-directed velocities as a function of ΔV.

It is evident from Fig. 8 that, under certain conditions, the influence of SRP is such that precession will have taken place at a sufficient rate for this perturbation alone to have caused full evolution prior to a particle deorbiting. This situation does not arise however in the evolution of the ascending node. Only under extreme velocity dispersion conditions might it be expected that SRP will cause a noticeable influence in Ω. It should be recalled that these figures relate to the maximum possible effect caused by SRP.

Evaluation of Breakup Scenarios

Using the methodology just adopted, it is possible to define the characteristic time T_{char} required for a group of particles to have achieved full evolution. Defining T_{char} to be specifically the ratio {orbit lifetime}/{time to form a band}, for the chaotic assumption we require T_{char} to be greater than unity.

In a general fragmentation event velocities can be expected to be distributed over a range of angles, not necessarily and indeed unlikely, isotropically. Figure 10 shows how the evolution for a particle, having an area-to-mass ratio of 0.025, is affected if the velocity vector arising from the fragmentation event is either directly opposed to, or in the direction of, the instantaneous velocity vector of the parent object. As before, these simulations relate to average solar activity. It is now apparent, particularly for the lower altitude shown, that the value of T_{char} is significantly changed. The scaling effect caused by area-to-mass ratio just noted, plus the potential dependence of velocity imparted to a particle upon the particle's mass, implies that for a closer understanding of how well microscopic chaos represents the debris environment specific models for a breakup events must be considered.

Two different types of debris generation events, explosions and collisions, are considered. The classification for objects is by their mass on a logarithmic scale, typically with around 50 mass bins per event. A few sample results were also obtained with much greater mass resolution (300 mass bins), but these did not materially change the results reported here.

In each of the next cases, an isotropic dispersion of particles, relative to the parent object, was not assumed intrinsically, because the way in which particles evolve as a result of the direction of their dispersion velocity, in regard to T_{char}, is highly nonlinear. Individual results were processed on evolution into a specific range of dispersion angles. A simplified summary result assuming isotropic dispersion is also evaluated.

Explosive Breakup Events

A number of different models have been proposed in the literature to model explosive breakup of an object, mainly following the pioneering work of Bess.[15] These are generally however all of a similar logarithmic form given by the cumulative number of objects exceeding a specific mass. The typical form is

$$N_e = a_e \cdot M_{\text{tg}} \cdot \exp\left(b_e \cdot m_g^{c_e}\right) \tag{7}$$

N_e is the number of objects generated in the explosion whose mass in grams exceeds m_g; a_e, b_e, and c_e are empirically determined constants, which in some models do and in others do not depend on the mass range considered. A review of this type of model is included in Ref. 11. The values adopted for the baseline simulation here are the following: a: 5×10^{-4}; b:0.04; and c: 0.5.

The velocity distribution for the objects was assumed to be related to the mass of the object. The form of this correlation is given by

$$\Delta V_e = 0.2154 \cdot m_e^{-0.159} \tag{8}$$

where m_e is now the mass in kilograms. This formulation was taken from Ref. 11, with data based on the experiments of Tan.[16] Other analyses[17] are not conclusive on the correlation between mass and velocity imparted, although the correlation has been assumed here.

Reynolds[18] has provided a different relationship for breakup events, independent of the means by which the breakup was induced. This formulism, based on size rather than mass, is given by

$$\log(\Delta V) = -0.676 \cdot [\log(d)]^2 - 0.804 \cdot \log(d) - 1.514 \tag{9}$$

This relationship, together with the relationship between ballistic coefficient and mass given by McKnight et al.,[19] was used for comparative purposes. The drag coefficient was assumed by McKnight to be constant over the altitude range, with a value of 2.2. The ballistic coefficient for a fragment of mass m_f is then given by

$$BC = k \cdot m_f^{-\alpha} \tag{10}$$

Whereas a range of parameters for k and α is provided by McKnight, the specific values assumed in the calculations here are k: 0.1 and α: 0.3.

For an explosion of a 1000-kg object, Fig. 11 shows the variation of T_{char} with fragment mass, when the velocity for each fragment produced, is assumed to be along the instantaneous velocity of the parent object at the moment of the explosion. The conditions for this event are of an object initially in an orbit of eccentricity of 0.001, with an inclination of 50 deg to the equator. This inclination is assumed next for all of the results presented and can, therefore, at appropriate altitude be considered as an ISS-type orbit. In Fig. 11 the orbit altitude at which the fragmentation, depicted by Eq. (8), took place is indicated. It is apparent from this figure that for velocity increments applied along the instantaneous velocity vector all objects created above 400 km, for an atmosphere assumed to be associated with average solar active conditions, will propagate forward to a fully evolved structure before deorbiting. At 400 km it is only the smaller particles that can be expected to evolve. Figure 12 shows a comparison for the same initial event conditions, for a cloud generated by the velocity relationship given by Eq. (9), in comparison to that given by Eq. (8). It is apparent that a greater fraction of fragments will evolve under the Reynolds model. Figure 13 shows results for the case where the velocity increment is directly opposed to the instantaneous velocity vector at fragmentation. It is now apparent that it is only at the higher altitudes, 800 km and above, where some particles evolve to $T_{\text{char}} > 1$. Further, it is only for a subset of particles, with mass greater than approximately 1 kg, that do so evolve, with the smaller particles being prematurely removed from the debris cloud.

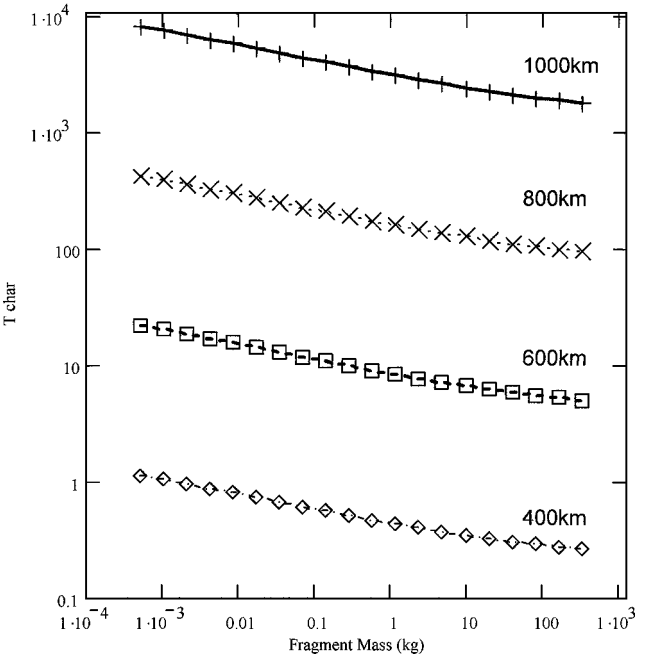

Fig. 11 T_{char} as a function of fragment mass for explosive fragmentation with forward-directed velocity.

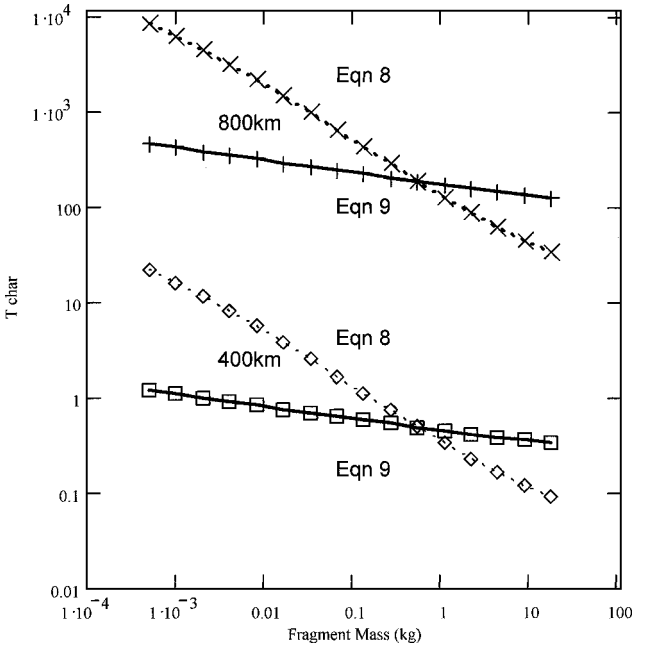

Fig. 12 Comparison of the effects of velocity models, given by Eqs. (9) and (10), upon T_{char} for explosive fragmentation with forward-directed velocity.

Using Eq. (7), it is possible to calculate the fraction of particles in a particular mass bin. Table 1 compiles such data for the total fraction of particles, which will evolve with $T_{\text{char}} > 1$ for an explosion, given the preceding assumptions, with the velocity model of Jehn, if the cloud that forms is isotropically dispersed. Angular binning in 10-deg steps for the dispersion velocity was adopted for these calculations. Further discussion of this table is given next following a description of the properties of a debris cloud, generated by a collision event.

Collision-Induced Fragmentation

To evaluate the state of evolution of specific breakup events, the model of McKnight[19] was used to provide data on the relationship

Table 1 Fraction of fragments having T_{char} >1, for target orbit at 50 deg (see text for details)

Altitude, km	Collision induced: fraction evolving	Explosion induced: fraction evolving
400	0.40	0.23
600	0.48	0.50
800	0.49	0.77
1000	0.50	0.88

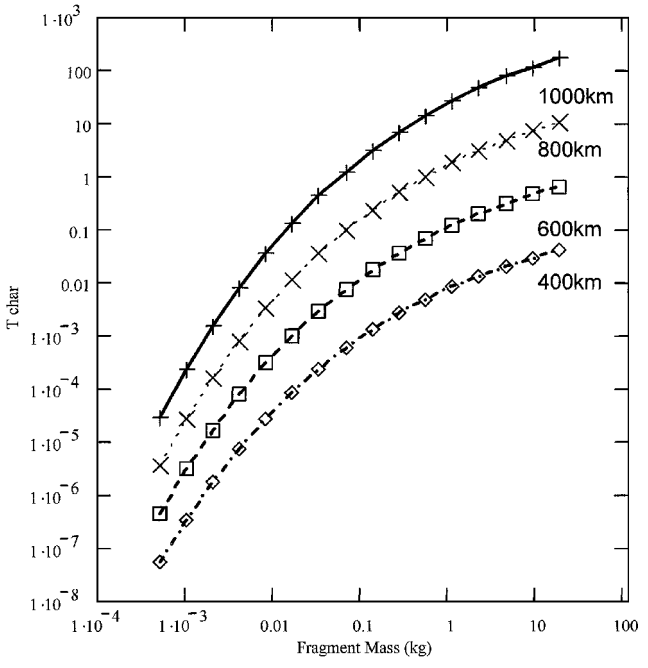

Fig. 13 T_{char} as a function of fragment mass for explosive fragmentation with rearward-directed velocity.

for dispersion velocity and particle size. In McKnight's model the cumulative number of particles above a given size is determined by a power law. The experimental data used to provide values for best-fit parameters for this power law spanned nearly two orders of magnitude in impact energy.

The cumulative number of particles N_c whose mass is greater than m_f is given by McKnight to be

$$N_c = a_c \cdot (m_f/M_t)^{-b_c} \tag{11}$$

with a_c: 0.4645 and b_c: 0.7.

This model, as a result of the power law nature, requires some minimum cutoff mass, given by McKnight to be dependent on both the kinetic energy E of the collision and the ratio of the projectile m_p to target masses M_t:

$$m_c = 3.3 \times 10^{-10} \cdot (m_p/X \cdot m_t) \cdot \sqrt{E} \tag{12}$$

X is a parameter used to indicate the type of impact: low values to represent collision with loosely coupled components, such as solar arrays, and higher values (maximum of 1) for closely coupled components.

The velocity distribution function v_c for the particles having a mass m_f created in the collision is then directly proportional to the relative speed of impact V_{imp} and a factor dependent on m_c:

$$v_c = 1.3V_{imp} \cdot \sqrt{[m_c/(m_c + m_f)]} \tag{13}$$

Figure 14 shows the dependence of T_{char} for fragment masses if the velocity imparted to the fragment is directed along the instantaneous

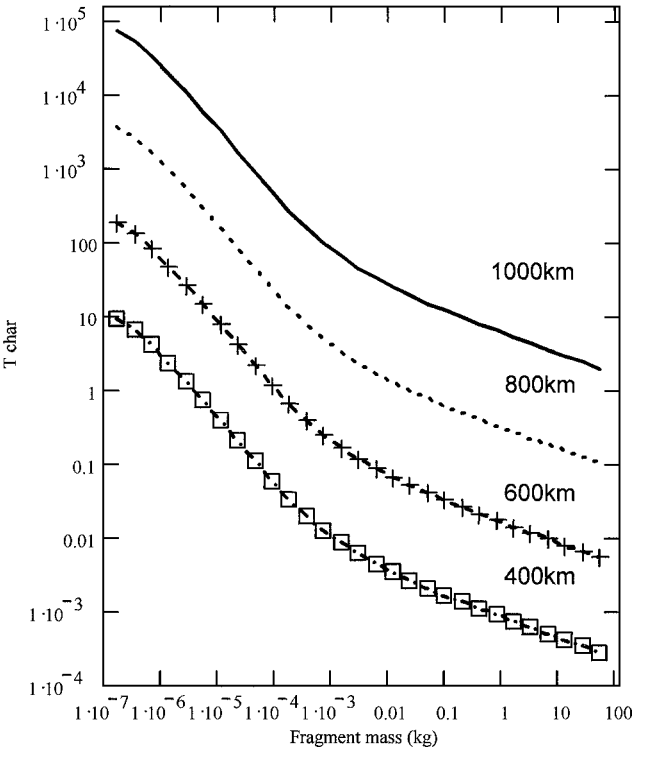

Fig. 14 T_{char} as a function of fragment mass for collision fragmentation with forward directed velocity.

velocity vector of the target object, at impact. To obtain these results, it was assumed that a target object of 1000 kg was impacted by a 10-kg projectile, at a relative velocity of 8000 m/s. As in the earlier sections, the initial orbit was taken to be nearly circular with an eccentricity of 0.001 and inclination 50 deg.

It can be seen from this curve that for this particular case, with a positive increment in velocity applied at perigee, it is the largest particle sizes at low altitude, that fail to evolve. Although this situation arises from the combination of the variation in ballistic parameter $(C_d \cdot A/m)$ and the velocity dispersion, it is principally the low dispersion velocity for the largest fragments that cause this trend. This trend is indeed evident from the earlier figures (e.g., Figs. 5 and 11), where low velocity dispersion results in particles decaying from orbit prior to evolution simply because the rate of dispersion is proportional to the change in the semimajor axis raised to some power, which depends upon the harmonic term of the gravitational potential.

In Fig. 15 results are shown for the case where the velocity increment is not directed along the instantaneous velocity vector. The marked variation in resultant T_{char} as a function of particle mass is evident from simply considering a velocity vector directed either 10 deg ahead of, or 10 deg behind, the radial direction. It is now apparent that the lower mass particles show the lowest values of T_{char}. A maximum T_{char} is typically evident as a function of fragment mass in any collision-induced breakup event, which can in certain circumstances result in an enhanced fraction of midmass particles fully evolving. The results for the lowest mass particles are caused by the high velocity imparted to these particles, which acts to reduce their final value of a significantly. Indeed for any given impact the degree to which these smaller particles become essentially filtered out from the overall original mass spectrum is dependent on the direction at which they were ejected relative to the initial velocity.

Analysis was undertaken to investigate the degree to which particle filtering takes place as a result of the initial direction of $\Delta V (= v_c)$ and the type of impact event. The particular case of a 400-km, near-circular orbit at 50-deg inclination was taken for the target object, having a mass of 1000 kg. In each case a constant mass projectile of 64 kg was impacted upon the target. The impact occurred at various impact speeds, as indicated in Fig. 16. Variation in impact conditions can also be characterized by the energy-to-mass

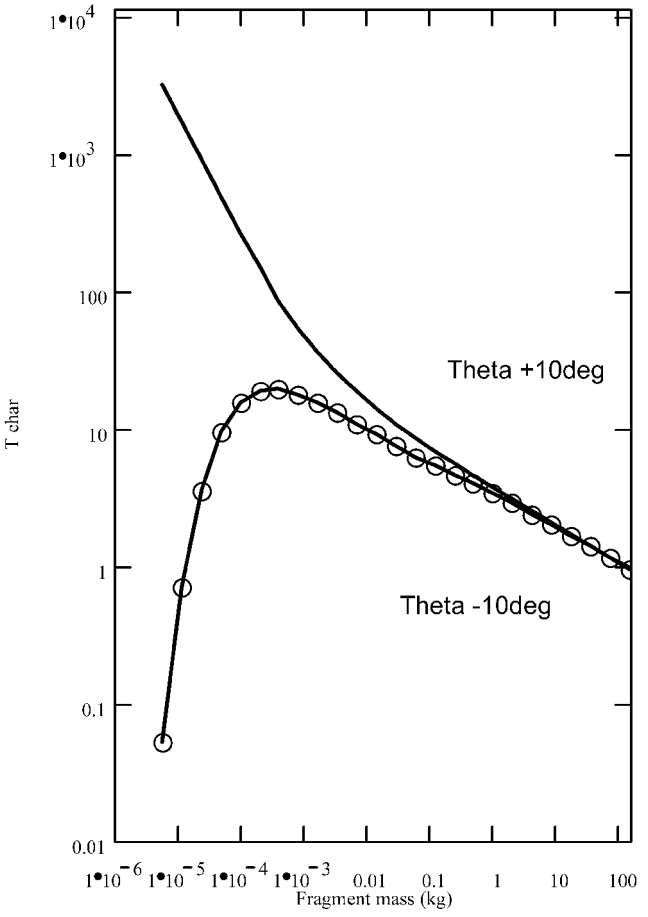

Fig. 15 T_{char} as a function of fragment mass for collision fragmentation with forward-directed velocity and behind instantaneous velocity vector at fragmentation.

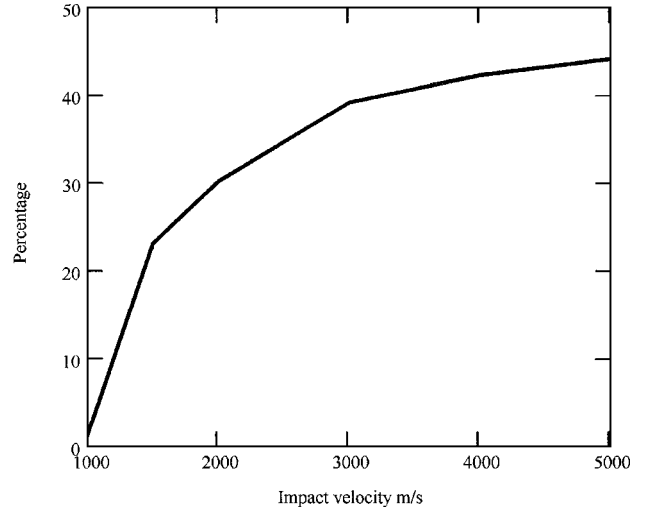

Fig. 16 Percentage of particles evolving with T_{char} >1 for a 64-kg projectile impacting a 1000-kg target in an orbit incline to the equator of 50 deg, at an altitude of 400 km.

ratio (EMR) defined as EMR $= 0.5 \cdot m_p v_{imp}^2 / M_t$. In Fig. 16 results correspond to an EMR between 32 and 800 J/gm.

The data plotted in Fig. 16 indicate that at this altitude, at the lowest impact energy, no particles evolve to form a band structure. As the energy of the impact increases, the fraction of the total number of particles, which do evolve, rises to a maximum of 44%. From the earlier results of Fig. 15, it is apparent that not all sizes of particles created in the collision will evolve. Indeed at this low altitude there will be a maximum size of object that will have $T_{char} > 1$.

Table 2 Maximum mass for fragments having T_{char} >1, for target orbit at 50 deg (see text for details)

Altitude, km	Maximum mass for evolving fragments			
	Collision			
	E_{coll} 64 J/kg	E_{coll} 320 J/kg	E_{coll} 1600 J/kg	Explosion
400	2×10^{-6}	10^{-4}	10^{-3}	All
600	6×10^{-5}	10^{-3}	0.03	All
800	5×10^{-3}	0.25	16.3	All
1000	All	All	All	All

Discussion

In Tables 1 and 2 data are collected for differing conditions appertaining to both collisions and explosions at different altitudes. In compiling these summary tables it has been assumed that the fragments are dispersed isotropically for both types of event. Mass and particle fraction data were evaluated in 10-deg intervals in velocity dispersion and then numerically integrated to give the data presented.

In Table 1 the fraction of the total number of particles produced in a fragmentation event, which evolve with $T_{char} > 1$, is indicated. For the collision data a collision energy, with an EMR having a value of 320 J/g, somewhere in the midrange of the empirical data used by McKnight to formulate his breakup model, is assumed. This collision impact was assumed to occur at a velocity of 8000 m/s. The comparison between explosions and collisions shows that there is a markedly different behavior for the two events. Collisions produce vast numbers of very low mass particles. Herein a specific value for a power law relationship has been adopted; however, most workers adopt similar models, albeit with varying cutoff values for the smallest particles produced and differing exponents in the power law relationship. It is these lowest mass particles that evolve fully in most collisions. However in a collision it is predominantly only the forward directed particles that evolve. As a result, even at the highest altitude of this study, 1000 km, a maximum of 50% of the particles do fully evolve. This effect is noticeable from the data presented in Fig. 15. In contrast under explosive breakup, rearward-directed particles can evolve, with the effect being again more apparent at higher altitude. Under these conditions it is the largest particles that evolve. As a result, as indicated in the table, a higher fraction of the total number of particles produced in the case of an explosion evolve.

These trends are confirmed in the data tabulated in the second table. Here the maximum mass for an evolving particle is indicated as a function of both altitude and collision energy. Results for three specific values of EMR are shown, again as a function of altitude. As the energy of the collision increases, within each case the velocity of the impact being constant at 8000 m/s, the mass of particles that evolve increases. It should be recalled from the preceding information that in the case of collisions it is predominantly the forward-directed particles that are evolving. Indeed it is this group of forward directed particles that identify the maximum mass particle that evolve. There is no maximum mass for an evolved particle size observed for the explosion induced breakup event, and hence a wider mass range of particles satisfies the criterion $T_{char} > 1$ for such breakups.

Conclusions

The presented data have shown that during the early phase in the evolution of a debris cloud it is important to include as a minimum the effects of J_2 and J_3. Failure to do so will overestimate the time required for a torus to form. This effect may influence the anticipated hazard posed to other satellites during the early phase of debris release.

The results that have been presented demonstrate a new methodology for evaluating debris cloud composition, namely what type of objects following which type of events are able to reach an evolutionary stage of microscopic chaos. It is apparent that there is a highly nonlinear behavior in the dependence of T_{char} on velocity dispersion angle relative to the initial object that fragments. Care should therefore be taken when the hazard posed to a satellite is based on isotropic dispersion during fragmentation.

The results confirm that for the smaller size particles the assumption of chaos is well founded for orbits above 400 km, although there will be selection effects in the nature of the mass distribution of these particles. There will however clearly be some fragmentation events from which the resulting cloud will not achieve the required state of evolution for DSMC evaluation. The DSMC method is not appropriate as an analysis tool for larger debris object impacts, which have themselves been created as a result of collision, upon target vehicles at low altitudes.

References

[1]Bird, G. A., *Molecular Dynamics and Direct Simulation of Gas Flows*, Oxford Engineering Series 42, Oxford Univ. Press, Oxford, 1994.

[2]Wang, L., and Stark, J. P. W., "Direct Simulation of Space Debris Evolution," *Journal of Spacecraft and Rockets*, Vol. 36, No. 1, 1999, pp. 114–123.

[3]Wang, L., and Stark, J. P. W., "DSMC Predictions of the Population Growth of Space Debris," *Rarefied Gas Dynamics 20*, edited by Ching Shen, Peking Univ. Press, Beijing, 1996, pp. 233–238.

[4]Wang, L., Stark, J. P. W., and Crowther, R., "DSMC Simulation of Collision Frequency of Orbital Debris," International Academy of Astronautics, Paper 95-IAA.6.4.02, Oct. 1995.

[5]Stark, J. P. W., "DSMC Simulation of Space Debris," *Rarefied Gas Dynamics 19*, edited by J. K. Harvey, and G. Lord, 1994, pp. 1373–1379.

[6]Wang, L., and Stark, J. P. W., "DSMC Simulation of Space Debris and Comparison with LDEF Impact Experiment," Second European Conf. on Space Debris, ESA SP 393, Noordwijk, The Netherlands, 1997, pp. 333–338.

[7]Wang, L., and Stark, J. P. W., "DSMC of Space Shuttle Space Debris Flight Damage," International Academy of Astronautics, Paper 98-IAA.6.4.02, Oct. 1998.

[8]King-Hele, D. G., *Satellite Orbits in an Atmosphere*, 1st ed., Blackie, Glasgow, Scotland, U.K., 1987, pp. 66–76.

[9]Housen K. R., "An Analytic Model of Debris Evolution for Fragmented Artificial Satellites," Boeing Rept., D180-32710-1, Aug. 1991.

[10]McKnight, D., and. Lorenzen, G., "Collision Matrix for Low Earth Orbit Satellites," *Journal of Spacecraft and Rockets*, Vol. 26, No. 1, 1989, pp. 90–94.

[11]Jehn, R., "Dispersion of Debris Clouds from In-Orbit Fragmentation Events," *ESA Journal*, Vol. 15, No. 1, 1991, pp. 63–77.

[12]Groves, G. V., "Motion of a Satellite in the Earth's Gravitational Field," *Proceedings of the Royal Society*, Vol. 254, No. 1, 1959, pp. 48–65.

[13]Aksnes, K., "Short Period and Long Period Perturbations of a Spherical Satellite due to Direct Solar Radiation Pressure," *Celestial Mechanics*, Vol. 13, No. 2, 1976, pp. 89–104.

[14]McKnight, D., "A Phased Approach to Collision Hazard Analysis," *Advances in Space Research*, Vol. 10, No. 3, 1990, pp. 385–395.

[15]Bess, T. D., "Mass Distribution of Orbiting Man-Made Space Debris," NASA TN D8108, Dec. 1975.

[16]Tan, A., "Estimation of Velocity Perturbations in Satellite Fragmentation Events," NASA/ASEE Final Rept., NASA/ASEE Summer Faculty Fellowship Programme-Johnson Space Center, Aug. 1988.

[17]Culp, R. D., and Madler, R. A., "Simulation of Satellite Breakups," AIAA Paper 86-2220, Oct. 1986.

[18]Reynolds, R. C., "A Review of Orbital Debris Environment Modelling at NASA/JSC," AIAA Paper 90-1355, Oct. 1990.

[19]McKnight, D., Maher, R., and Nagl, L., "Refined Algorithm for Structural Breakup due to Hypervelocity Impact," Hypervelocity Impact Society Symposium, Paper 082, Oct. 1994.

J. C. Taylor
Associate Editor